Microstructure and magnetic properties of atmospheric plasma sprayed Fe-40Al coating obtained from nanostructured powders

Bo Song, Shujuan Dong, Nour-Eddine Fenineche, Eric Aubry, Thierry Grosdidier, Hanlin Liao, Christian Coddet

▶ **To cite this version:**

Bo Song, Shujuan Dong, Nour-Eddine Fenineche, Eric Aubry, Thierry Grosdidier, et al.. Microstructure and magnetic properties of atmospheric plasma sprayed Fe-40Al coating obtained from nanostructured powders. Applied physics. A, Materials science & processing, 2013, 113 (3), pp.787-792. 10.1007/s00339-013-7593-7 . hal-01501659

HAL Id: hal-01501659
https://hal.univ-lorraine.fr/hal-01501659v1

Submitted on 23 Jul 2024

HAL is a multi-disciplinary open access archive for the deposit and dissemination of scientific research documents, whether they are published or not. The documents may come from teaching and research institutions in France or abroad, or from public or private research centers.

L'archive ouverte pluridisciplinaire **HAL**, est destinée au dépôt et à la diffusion de documents scientifiques de niveau recherche, publiés ou non, émanant des établissements d'enseignement et de recherche français ou étrangers, des laboratoires publics ou privés.

Distributed under a Creative Commons Attribution - NonCommercial 4.0 International License

Microstructure and magnetic properties of atmospheric plasma sprayed Fe–40Al coating obtained from nanostructured powders

Bo Song · Shujuan Dong · Nour-Eddine Fenineche · Eric Aubry · Thierry Grosdidier · Hanlin Liao · Christian Coddet

Abstract Amorphous and nanocrystalline materials have attracted much interest in the field of new materials design because of their excellent mechanical and physical properties as well as their magnetic properties. In this work, Fe–40Al coatings were prepared from nanostructured feedstock with a very low degree of order using atmospheric plasma spraying. Scanning electron microscopy, X-ray diffraction, and magnetic measurements were used to investigate microstructure, phase structure, and magnetic properties of the coatings. The results showed that Fe–40Al coating presented a ferromagnetic character due to partial structure with a low degree of order and unmelted nanostructured particles retained from the feedstock. Moreover, the heterogeneous magnetic properties were found in the parallel and vertical direction of the coating.

1 Introduction

Iron aluminide intermetallic compounds have been widely studied because of their low cost, high ratio of strength to weight, and excellent resistance to oxidation, wear and corrosion [1, 2]. However, commercial application of these materials has been limited by their low ductility at room temperature and low mechanical strength above about 600 °C. Reducing the crystallite size to the nanometer range has been acknowledged as one efficient approach for improving the ductility of iron aluminide intermetallic compounds [3–5].

Iron aluminide alloy is also one of the typical magnetic materials [6–8]. It is recognized that the microstructure, as well as the grain size, essentially determines the magnetic properties. The deformed or disordered Fe–Al powder could show ferromagnetic properties at room temperature, even for the powder, the Al concentration of which is over 50 at.% [9]. In particular, the development of the nanocrystalline material provided an application prospect of soft ferromagnetic materials in magnetic devices such as transformers, inductive devices, etc. [10]. Due to the extremely small size of the grains, a large fraction of the atoms in these materials is located at the grain boundaries and thus the material might exhibit unusual physical properties, compared to those of conventional materials with microcrystalline grain size [11]. Mechanical milling (MA) technique is widely employed to produce nanostructured materials with non-equilibrium microstructures by bringing about significant disordering and internal lattice strain while reducing the size of the coherently diffracting domains down to the nanometer range, as described for FeAl material in several papers [3–5].

Considering that the nanostructured iron aluminide alloys have so many advantages for their applications, in this work, the nanostructured Fe–40Al powders with a very low degree of order were used as feedstock to deposit coatings by atmospheric plasma spray (APS), since APS is attractive in industry for its relatively high deposition efficiency and

B. Song (✉) · S. Dong · N.-E. Fenineche · E. Aubry · H. Liao · C. Coddet
IRTES-LERMPS, Université de Technologie de Belfort-Montbéliard, 90010 Belfort Cedex, France
e-mail: bo.song@utbm.fr
Fax: +33-03-84583286

S. Dong (✉)
e-mail: shujuan.dong@utbm.fr
Fax: +33-03-84583286

T. Grosdidier
LETAM, CNRS 3143, Université Paul Verlaine-Metz, Ile du Saulcy, 57012 Metz Cedex 01, France

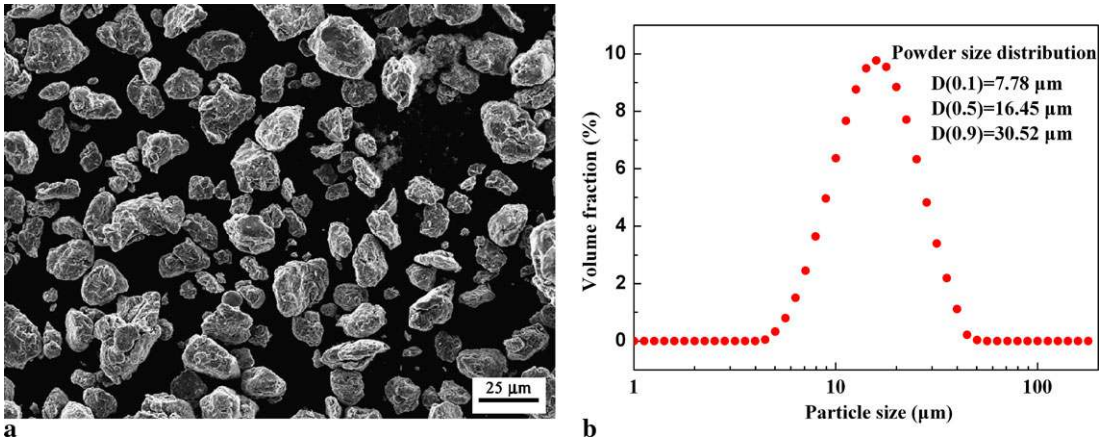

Fig. 1 (**a**) SEM observation and (**b**) size distribution of FeAl powder

low cost and high flexibility [12, 13]. The microstructure, phase structure, and magnetic properties of plasma-sprayed Fe–40Al coatings were studied in detail.

2 Materials and experimental procedures

The microstructure and the size distribution of the powder used as feedstock were shown in Fig. 1. The composition is Fe–40Al–0.05Zr (at.%) with 50 ppm B. These powders were fabricated by the atomization process under argon atmosphere and the milling process for 50 hours in a semi-industrial planetary ball mill (Retsch PM 400) developed by CEA-CEREM (Commissariat à l'énergie atomique-Centre d'étude et de recherches sur les matériaux) [14]. A capability of 10 kg of powder per batch was realized under a charge of 100 kg of carbon steel balls (diameter: 30 mm). With the rotation of the disc, the mounted vials on the planar disc moved in a circular and opposite direction compared to the disc rotation. All these operations are carried out under very specific conditions to limit contamination by the atmosphere or exogenous inclusions [14]. Hellstern et al. [15] and Suryanarayana [16] have in detail described the mechanism of formation of nanostructures by mechanical alloying, where nanocrystalline grains could be formed. In our work, resulting powders had granulometry sizes of 16 µm as the feedstock. Their gain sizes were estimated using X-ray diffraction as will be described.

Atmospheric plasma spraying using a Sulzer-Metco F4 plasma gun was employed to deposit FeAl coatings on Al substrates. Argon was used as both plasma-operating and powder carrier gas. Spraying parameters were set up as follows: arc current (600 A), arc voltage (65 V), primary plasma gas (Ar, 50 SLPM), secondary plasma gas (H_2, 10 SLPM), powder carrier gas (Ar, 3.8 SLPM). The plasma spray distance was fixed at 100 mm. The spraying torch was mounted on the flange of a robot and vertically moved in front of samples.

The microstructure of as-sprayed coatings was observed using optical microscopy (OM) and scanning electron microscope (SEM) equipped with energy dispersive X-ray spectroscopy (EDS, JEOL, JSM-5800LV, Japan) on cross-sections prepared using standard cutting and polishing techniques. The porosities and oxide contents of the as-sprayed coatings were estimated using an image analysis (IM) of the OM micrographs. More than five photographs randomly observed in the polished cross-section were averaged to evaluate the porosity and oxide content.

Magnetic properties such as coercivity (H_c) and saturation magnetization (M_s) were determined from M–H loops measured using a LakeShore (model 7300) vibrating sample magnetometer at room temperature. The measurements were realized with a magnetic field applied in the specimen plane and the normal direction of the samples. Specimen area was 0.125 cm^2. The maximum magnetic field was fixed at 10 kG.

XRD measurements were conducted on a Siemens diffractometer, operating with a cobalt anticathode ($\lambda =$ 1.78897 Å) at 35 kV and 40 mA and employing a scan rate of 10° min^{-1} in a scattering angular range (2θ) of 20–110°. The Williamson–Hall method is used to calculate some structural parameters from the XRD data, taking into account Co $K\alpha 1$ radiation, after $K\alpha 2$ stripping using the Rachinger method. The grain size and the average micro strain in the feedstock powders and coatings were estimated based on the modified Williamson–Hall method [17, 18]. The line broadening of a Bragg reflection $(hkl) - \beta_{hkl}$ is obtained by

$$\beta_{hkl} = \left[(\beta_{hkl})^2_{\text{measured}} - (\beta_{hkl})^2_{\text{instrumental}}\right]^{1/2}, \quad (1)$$

$$\beta_{hkl}\cos\theta_{hkl} = K\lambda/D + 4\varepsilon\sin\theta_{hkl}. \quad (2)$$

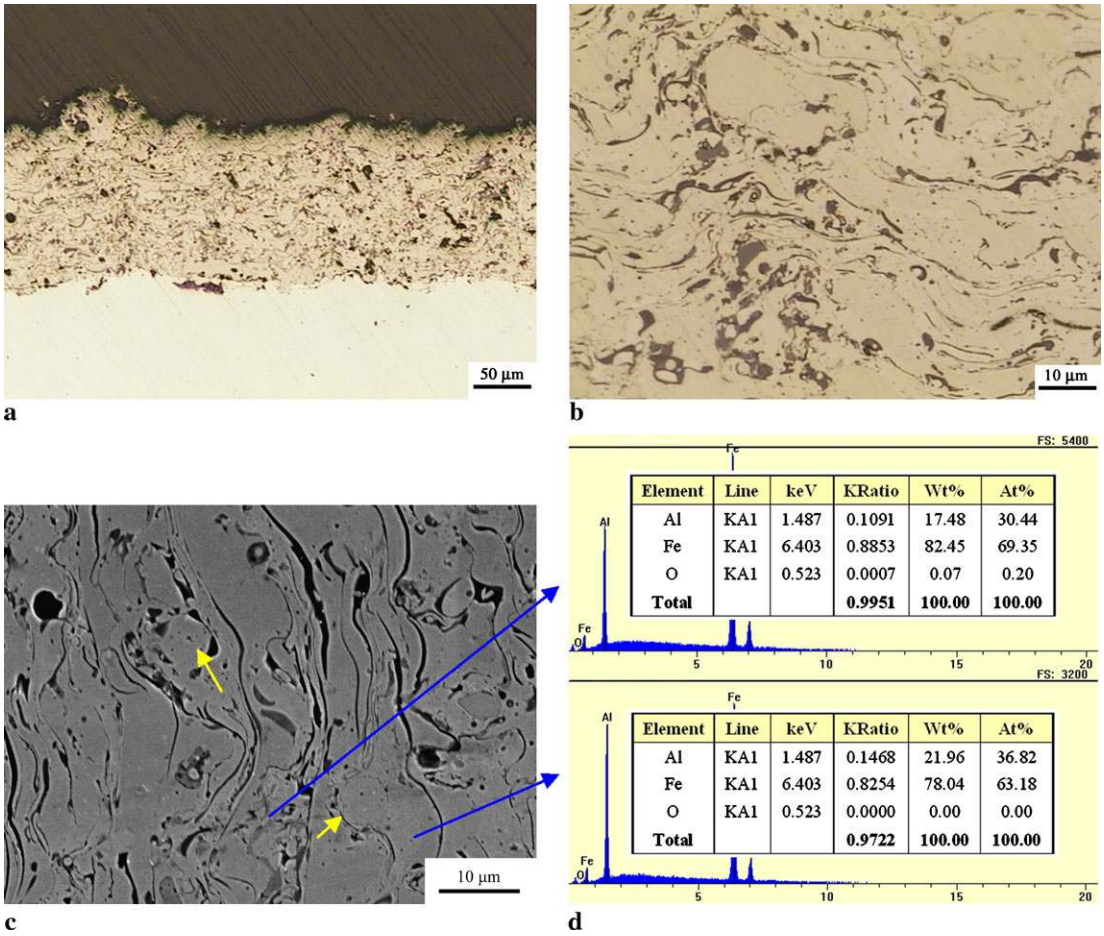

Fig. 2 OM observation of Fe–40Al coatings at (**a**) low magnification, (**b**) high magnification, (**c**) SEM observation and (**d**) the corresponding EDS analysis on the position marked with *blue arrows* in Fig. 2c

The Williamson–Hall equation is expressed in the above formula (2). Here, the shape factor K is constant 0.89, λ the X-ray wavelength, θ_{hkl} the Bragg angle with miller indices (h,k,l), and D the effective crystallite size normal to the reflection planes. Through plotting the value of $\beta_{hkl}\cos\theta_{hkl}$ as a function of $4\sin\theta_{hkl}$, the micro strain ε was estimated from the slope of the linear relation and the crystallite size from the intersection of the line with the vertical axis.

3 Results and discussion

3.1 Microstructure and phase analysis

Figure 2 displays typical cross-sectional images of plasma-sprayed Fe–40Al coatings. The coating thickness is about 150 µm as shown in Fig. 2a. It can be noted from the microstructure in Fig. 2b that the Fe–40Al coating was composed of pores, the fundamental FeAl phase, Fe_3Al phase and oxides which were confirmed by the SEM-EDS method as shown in Fig. 2c–d. Two of main contrasts correspond to FeAl phase and Fe_3Al phase. The statistic analysis of the porosity, Fe_3Al and oxide using image J free software yield 10.2 %, 2.8 %, and 2.4 %, respectively. The percentage of each component in the coating was consistent with that reported in another publication about FeAl coating [19]. Furthermore, it can be clearly observed that there exist many unmelted nanostructured Fe–40Al particles in the coating as marked with yellow arrows in Fig. 2c, which would affect the magnetic property.

Figure 3 presents the X-ray diffraction results of the ball milled powders and the as-sprayed coating. Indeed, only the fundamental peaks (110), (200) and (211) are visible in the X-ray diagram for both the powders and coatings. For completely ordered Fe40Al intermetallic, the fundamental peaks as well as superlattice peaks (100), (111) and (210) could be detected by XRD method. However, the superlattice peaks have almost completely disappeared. This implies that the significantly disordered state exists in the milled powders and coatings. Moreover, the fundamental peaks of Fe40Al phase in the coating present the asymmetric Bragg peaks, also suggesting its partially ordered structure [20]. This phe-

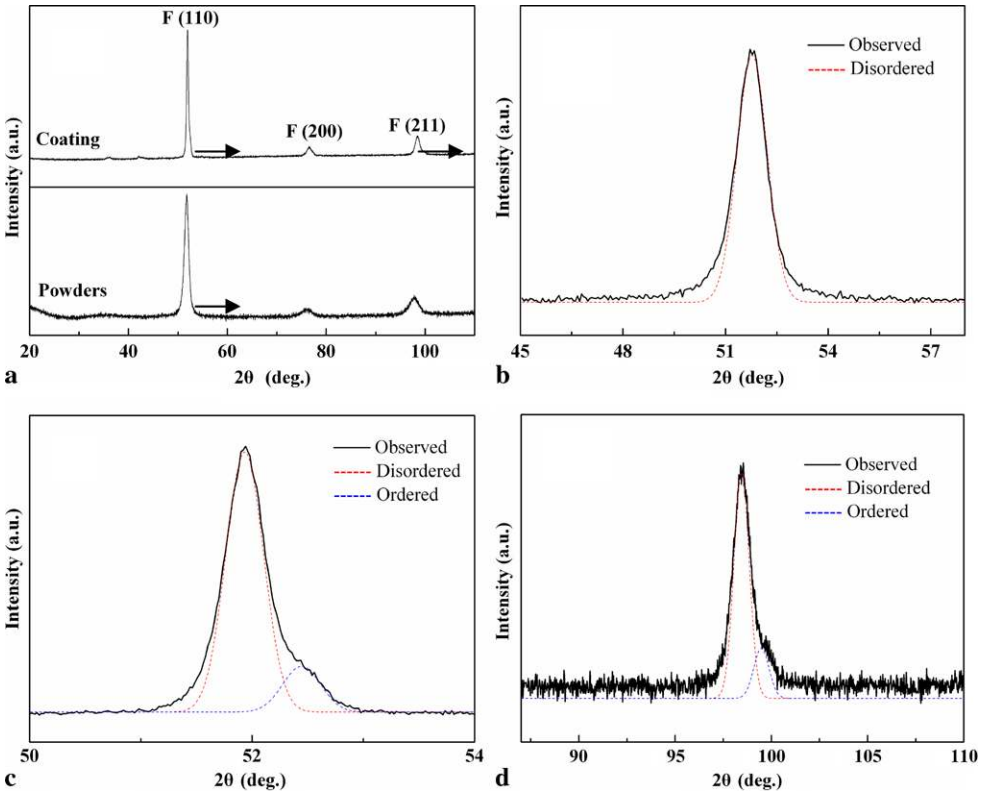

Fig. 3 (**a**) XRD patterns of the feedstock and the as-sprayed Fe–40Al coating, (**b**) the detailed profile of (110) peak of Fe–40Al powder, (**c**)–(**d**) the detailed profiles of (110) and (211) peaks of Fe–40Al coating, respectively. The *blue* and *red dash lines* indicate the fully ordered and the fully disordered Fe–40Al, respectively

nomenon is more obvious in Figs. 3c–d, which show the details of the fundamental (110) and (211) peaks of Fe40Al phase in the coating. In these three diagrams, the fundamental Bragg peaks of Fe40Al in the coating were fitted by the superposition of the ordered B2 curve and the disordered bcc (solid solution) curve as indicated by the blue and red dash lines, respectively. This fitting process is based on the fact that the fully disordered Fe40Al phase and the fully ordered one have the lattice parameters of 0.2925 nm and 0.2897 nm, respectively [21].

The resolution of the Bragg peaks for the disordered and ordered phases allows an estimation of the ordered volume fraction (V_{ordered}/V) from XRD profile analysis. The ordered fraction can be estimated from the fundamental Bragg peak intensities following the formula [20]:

$$V_{\text{ordered}}/V = I_{B2-hkl}/(I_{\text{bcc}-hkl+} + I_{B2-hkl}). \tag{3}$$

By calculating V_{ordered}/V estimated from (110) and (210) fundamental Bragg peaks, the result can be obtained that the Fe40Al coating consists of about 86 vol.% bcc (body-centered cubic) Fe (Al) solid solution phase. And only about 14 vol.% B2 phase was produced during the APS process. In other words, the degree of order is about 0.14.

On the other hand, the bcc lattice parameters of the powders and coatings could be calculated according to the formula (4) known as Bragg's law and formula (5) combined with the XRD data. The calculation results of the lattice parameters are 0.2916 and 0.2908 nm for the powders and coatings, respectively. These results are consistent with those about the degree of order estimated by the formula (3), because the degree of order increases with the increase in the lattice parameter [20].

$$2d_{hkl}\sin\theta = n\lambda, \tag{4}$$

$$d_{hkl} = a/\sqrt{h^2+k^2+l^2}. \tag{5}$$

Compared with the XRD peaks of the atomized powders [21, 22], the XRD peaks of the milled powders exhibit a broadening phenomenon and some decrease in the intensity, which are related with the development of both nanocrystalline structure and lattice strain in the powder particles. Moreover, the peaks of the coating are narrower than those of powders, implying that grain growth occurred in the particle melting process during plasma spraying. The grain size and the average micro strain in the powders and coatings were estimated based on the modified Williamson–Hall method as described in Sect. 2.

From the analysis results in Fig. 4, the result can be obtained that the size of coherent diffraction domains and the lattice strain of the feedstock are about 15 nm and 5.8×10^{-3}, respectively. These results agree with the reported data of the milled FeAl in other literature [4, 22]. For the coating, the coherent diffraction domain size and the lattice strain correspond to about 53 nm and 3.8×10^{-3},

respectively. The increase in coherent diffraction domains and the decrease in lattice strain were attributed to the particle melting process during the coating deposition process. Some structural defects, such as quenched-in vacancies and dislocation loops or anti-site atom pairs, could be eliminated by this heating process.

3.2 Magnetic characterization

The magnetic measurements were carried out from the parallel and vertical direction of the coating, as illustrated in Fig. 5.

Figure 6 shows the hysteresis loops of Fe–40Al coatings corresponding to the parallel and vertical direction. It can be found that the magnetic properties are sensitive to the direction of the coating, although Fe–40Al coating presents a ferromagnetic character in the two directions. In the parallel direction (Fig. 6a), a low coercivity (H_c) and a high saturation magnetization (M_s) were obtained, which confirmed that the anisotropy is in-plane of the coating. The saturation magnetization value is 16 emu/cm^2. The inset window shows the enlargement part of magnetization curves in the low magnetic field from −50 G to 50 G. The coercivity value is about 53 G. The low H_c and the high M_s values could be explained by the degree of order (0.14) and grain size (53 nm) of Fe–40Al coating. According to Besnus's results [9], the magnetic properties of the Fe–Al system strongly depend on the order state. And Apinaniz's results [24] confirmed the fact that the disorder degree increases the magnetism of the alloy compared with the ordered structures. The ordered Fe–Al alloys are known to be paramagnetic at room temperature when Al concentration is over 33 at.%. However, they become ferromagnetic at room temperature if the local atomic environment in these paramagnetic alloys is altered by deforming or disordering them, even though Al concentration is over 50 at.%.

In the vertical direction of the coating (Fig. 6b), the magnetic saturation is not achieved within the measurement range of magnetic field. Relatively speaking, it is more difficult to be magnetized. The inset window shows the enlargement part of magnetization curves in the magnetic field from −100 G to 100 G. Compared with the H_c (53 G) value in the parallel direction, it changes into about 125 G in the vertical direction. Moreover, it can be noted from the demagnetization curves that different remanence (M_r) values are recorded. The M_r value in the parallel direction is about 2.3 emu/cm^2, while it is about 0.3 emu/cm^2 in the vertical direction.

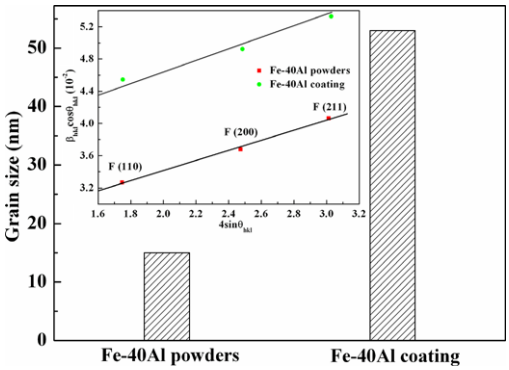

Fig. 4 Mean grain size of Fe–40Al powders and coatings. The *inset* window shows the corresponding Williamson–Hall plots

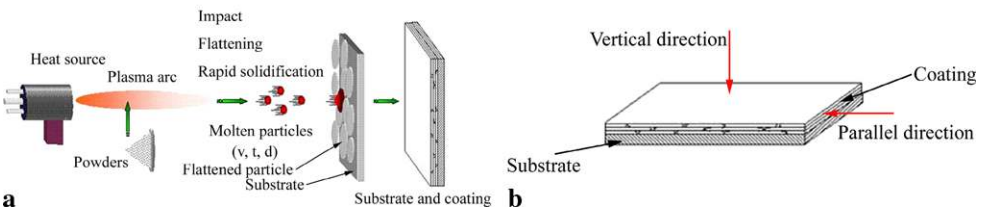

Fig. 5 (**a**) Diagram of the principles of atmospheric plasma spray technology [23] and (**b**) the detailed information of the coating

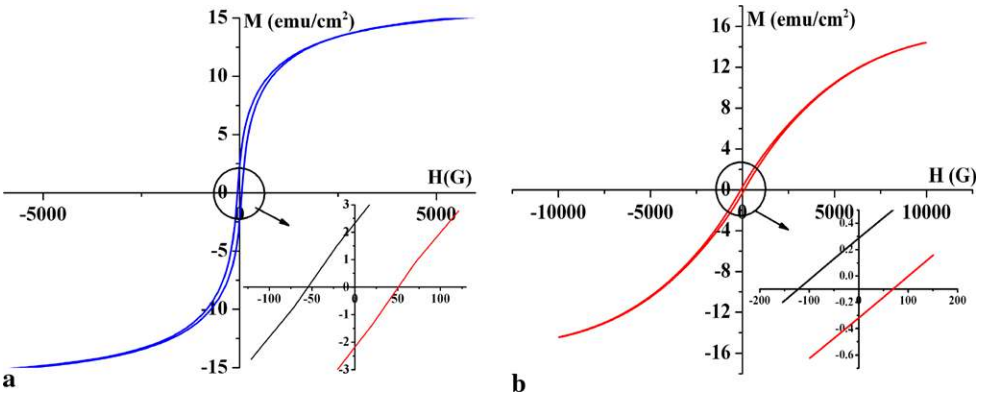

Fig. 6 Hysteresis loops corresponding to the (**a**) parallel and (**b**) vertical direction of Fe40Al coating

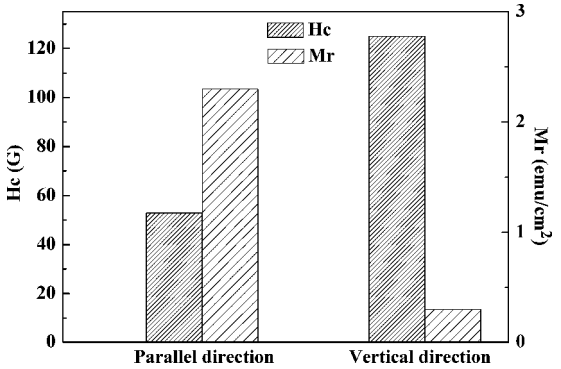

Fig. 7 Comparison of coercivity H_c and remanence M_r in two directions of the coating

From the comparison results of H_c and M_r values in Fig. 7, it is clear that although the remanence in the vertical direction is smaller than that in the parallel direction, it still needs the greater coercivity to demagnetize in the vertical direction of Fe40Al coating. Accordingly, the coatings in the parallel direction are suitable for soft magnetic applications than that in vertical direction. This heterogeneous magnetism is related to the structural features in the coating as illustrated in Fig. 5. Indeed, during the APS process, the molten and semi-molten droplets with a high speed impact into the substrate and flatten, rapidly solidify, and form one layer. Many layers accumulate to form a coating. In the parallel direction, each layer composed of individual splats could be like "sheet metal", which minimizes the magnetic exchange energy. In the vertical direction, the coating is composed of many layers. According to Li's work [25], the coating plasma-sprayed by the conventional route has a porous lamellar structure with limited interface bonding between the layers, and the maximum mean bonding ratio is about 32 %. This lower bonding ratio would lead to a different magnetic behavior in the vertical direction. This effect can be proved by the results of the previous study [26] about the effect of porosity in the coating on the coercivity. The predicted magnetic properties correlated with the coating porosity were obtained using artificial neural network. The increase of coercivity versus porosity level is explained by the fact that the porosity acts against the continuity of magnetic properties through the coating structure. These porosities are considered as defects anchoring Bloch walls and involving consequently an increase of coercivity [26]. Therefore, the limited interface bonding in the vertical direction can mainly be responsible for the larger coercivity, which is not very suitable for soft magnetic materials.

4 Conclusions

Atmospheric plasma spraying was employed to deposit Fe–40Al coating from the nanostructured feedstock with a very low degree of order. The as-sprayed coating is composed of the pores, the fundamental FeAl phase, Fe_3Al phase and the oxides. The coating has a degree of order of 0.14 and grain size of 53 nm. The coherent diffraction domains increase and the lattice strain decreases after the deposition process. A low coercivity and a high saturation magnetization were obtained due to the low degree of order. The heterogeneous magnetism in the parallel and vertical direction corresponds to the lamellar structure of the coating.

Acknowledgements The authors also gratefully thank S. Lamy and O. Ribet for their help in the sample characterization.

References

1. P. Juzoń, M. Ziemnicka, S. Chevalier, K. Przybylski, J.P. Larpin, Appl. Surf. Sci. **253**, 4928 (2007)
2. S.C. Vogel, F. Stein, M. Palm, Appl. Phys. A **99**, 607 (2010)
3. Z.H. Zhang, Y.Z. Zhou, E.J. Lavernia, J. Alloys Compd. **466**, 189 (2008)
4. S. Gialanella, X. Amils, M.D. Baro, P. Delcroix, G. Lecaer, L. Lutterotti, S. Surinach, Acta Mater. **46**, 3305 (1998)
5. G. Valdrè, G.A. Botton, L.M. Brown, Acta Mater. **47**, 2303 (1999)
6. C. Mangler, C. Gammer, K. Hiebl, H.P. Karnthaler, C. Rentenberger, J. Alloys Compd. **509**, S389 (2011)
7. R. Brajpuriya, P. Sharma, S. Jani, S. Kaimal, T. Shripathi, N. Lakshmi, K. Venugopalan, Appl. Surf. Sci. **257**, 10 (2010)
8. R. Bernal-Correa, A. Rosales-Rivera, P. Pineda-Gómez, N.A. Salazar, J. Alloys Compd. **495**, 491 (2010)
9. M.J. Besnus, A. Herr, A.J.P. Meyer, J. Phys. F **5**, 2138 (1975)
10. A.R. Yavari, D. Negri, J. Metastable Nanocryst. Mater. **1**, 63 (1999)
11. L. Del Bianco, A. Hernando, E. Bonetti, E. Navarro, Phys. Rev. B **56**, 8894 (1997)
12. S.J. Dong, B. Song, B. Hansz, H.L. Liao, C. Coddet, Mater. Lett. **66**, 289 (2012)
13. S.J. Dong, B. Song, B. Hansz, H.L. Liao, C. Coddet, Appl. Surf. Sci. **257**, 10828 (2011)
14. F. Moret, R. Baccino, P. Martel, L. Guetaz, J. Phys. IV **6**, 281 (1996)
15. E. Hellstern, H.J. Fecht, C. Garland, W.L. Johnson, in *Multicomponent Ultrafine Microstructures*, ed. by L.E. McCandlish, D.E. Polk, R.W. Siegel, B.H. Kear, vol. 132 (Mater. Res. Soc., Pittsburgh, 1996), pp. 137–142
16. C. Suryanarayana, Prog. Mater. Sci. **46**, 124 (2001)
17. G.K. Wiliamson, W.H. Hall, Acta Mater. **1**, 22 (1953)
18. H.P. Klug, L.E. Alexander, *X-Ray Diffraction Procedure for Polycrystalline and Amorphous Materials* (Wiley, New York, 1974)
19. G. Ji, T. Grosdidier, F. Bernard, S. Paris, E. Gaffet, S. Launois, J. Alloys Compd. **434–435**, 358 (2007)
20. D. Negri, A.R. Yavari, A. Deriu, Acta Mater. **47**, 4545 (1999)
21. T. Grosdidier, A. Tidu, H.L. Liao, Scr. Mater. **44**, 387 (2001)
22. B. Song, S.J. Dong, P. Coddet, B. Hansz, T. Grosdidier, H.L. Liao, C. Coddet, J. Therm. Spray Technol. (2012). doi:10.1007/s11666-012-9840-4
23. B.S. Xu, S.C. Liu, *China Materials Engineering Dictionary: Surface Engineering* (Chemical Industry Press, Beijing, 2006)
24. E. Apinaniz, J.S. Garitaonandia, F. Plazaola, J. Non-Cryst. Solids **287**, 302 (2001)
25. C.J. Li, A. Ohmori, J. Therm. Spray Technol. **11**, 365 (2002)
26. M. Cherigui, S. Guessasma, N. Fenineche, C. Coddet, Mater. Chem. Phys. **9**(3), 186 (2005)